Highly Accelerated UV Stress Testing for Transparent Flexible Frontsheets

Michael D. Kempe, Peter Hacke, Joshua Morse, Michael Owen-Bellini, Derek Holsapple, Trevor Lockman, Samantha Hoang, David Okawa, Tamir Lance, and Hoi Hong Ng

***Abstract*—For flexible photovoltaic (PV) applications, the dominant material for the frontsheet is poly(ethylene-co-tetrafluoroethylene). As a fluoropolymer, it resists soiling by letting the water run off easily, is resistant to degradation by exposure to ultraviolet light, and is more mechanically durable than most fluoropolymers. To keep costs down, less expensive alternative polymers are desirable. In this study, highly accelerated ultraviolet light and heat stresses are applied to candidate materials, and the degradation kinetics are determined to provide information to evaluate their suitability for use in a PV application. Because of the uncertainty in service life prediction, the acceleration parameters are instead used primarily to evaluate the relevance of the applied stresses. Here, we find that the best materials are fluoropolymer based and that even when exposed to high irradiance at high temperatures, relatively little degradation is seen. For the 15 materials tested here, we found the Arrhenius activation energy for various degradation processes to be 39 $\pm$ 22 kJ/mol with a power law dependence on irradiance of 0.49 $\pm$ 0.22 with a negative correlation coefficient of -0.606 (i.e., more highly thermally activated processes are less dependent on the irradiance level). For frontside exposure, the most severe conditions used here (4 W/m^2/nm @340 nm, 70 °C, for 4000 h) were on average equal to about 11.4 y in Riyadh, Saudi Arabia when mounted with insulation on the backside. Thus, to get relevant amounts of ultraviolet exposure with unmodified commercial equipment ($\sim$0.8 W/m^2/nm @340 nm) requires extraordinarily long exposure times, especially if conducted at lower irradiance levels.**

***Index Terms*—Durability, flexible, frontsheet, polymer, reliability, ultraviolet.**

Manuscript received 5 October 2022; revised 2 February 2023; accepted 18 February 2023. Date of publication 27 March 2023; date of current version 20 April 2023. This work was supported in part by the National Renewable Energy Laboratory, operated by Alliance for Sustainable Energy, LLC, for the U.S. Department of Energy under Grant DE-AC36-08GO28308 and in part by the U.S. Department of Energy, Office of Energy Efficiency and Renewable Energy, Solar Energy Technologies Office as part of DuraMAT under Grant 32509. The views expressed in this article do not necessarily represent the views of the DOE or the U.S. Government. The U.S. Government retains and the publisher, by accepting the article for publication, acknowledges that the U.S. Government retains a nonexclusive, paid-up, irrevocable, worldwide license to publish or reproduce the published form of this work, or allow others to do so, for the U.S. Government purposes. *(Corresponding author: Michael D. Kempe.)*

Michael D. Kempe, Peter Hacke, Joshua Morse, Michael Owen-Bellini, Derek Holsapple, and Trevor Lockman are with the National Renewable Energy Laboratory, Golden, CO 80401 USA (e-mail: michael.kempe@nrel.gov; peter.hacke@nrel.gov; jbmorse8@gmail.com; michael.owenbellini@nrel.gov; derekhols31@gmail.com; trevorlockman13@gmail.com).

Samantha Hoang, David Okawa, Tamir Lance, and Hoi Hong Ng are with the SunPower Corporation, San Jose, CA 95134 USA (e-mail: Samantha.Hoang@maxeon.com; DOkawa@gmail.com; tamir.lance@maxeon.com; Hoihong.ng@maxeon.com).

Color versions of one or more figures in this article are available at https://doi.org/10.1109/JPHOTOV.2023.3249407.

Digital Object Identifier 10.1109/JPHOTOV.2023.3249407

I. Introduction

THERE are many photovoltaic (PV) applications where lighter-weight and/or bendable PV modules would be beneficial. This includes the curved surfaces of buildings, buildings with weight limitations, boats, automobiles, or other portable applications. In many of these cases, the bending will be only a single occurrence at installation, or the amount of bending, even if repeated, is not dramatic. The small amount of bending allows for some types of crystalline silicon cells to be used. Most commonly, this has instead been accomplished using thin film amorphous silicon (a-Si) or copper-indium-gallium-sulfide (CIGS) based PV materials on a metallic substrate. While being lightweight and highly flexible, a-Si has demonstrated efficiency limits and CIGS typically requires significant protection from moisture ingress to be durable. Crystalline Si modules (c-Si) are both of relatively higher efficiency and good durability and are available in large quantities at low cost. The only drawback to c-Si is that it is more brittle than thin-film PV technologies and thus less tolerant of bending. If one limits the applications to places where it is only bent once during initial placement, or in forms where the need for flexing is minimal, a well-constructed c-Si cell can withstand this minimal amount of bending. However, the removal of a low thermal expansion glass layer could increase the need for better strain relief to accommodate thermomechanical stresses, but this issue is the same for any flexible technology.

Here, we investigate 15 different candidate frontsheet materials for consideration in a bendable PV package (see Table I). This included experimental controls as industrially proven materials and unstabilized film formulations as known bad materials. Some of the films were fully engineered samples capable of passing the IEC 61730 safety qualification testing, whereas others were just one of the layers (e.g., a fluoropolymer top layer). Candidates were ranked from high to low cost and were exposed to varying conditions of temperature, humidity, and light intensity while being monitored for retention of optical properties.

The intent is not to conduct a comprehensive service life prediction on these materials. That would require a detailed compositional understanding and a mechanistic understanding of all degradation processes [3], [4] of more than just the degradation modes investigated here. Instead, we seek to get an understanding of the range and variability of degradation mechanisms for PV frontsheet materials to get a rough idea of the range and

TABLE I
CANDIDATE FRONTSHEET MATERIALS

#	Material Description	Cost	Selection Type
1	PETFE (Monolithic)	High	PETFE (Positive control)
14	PVDF (Monolithic)	High-Med	Non-PET option
15	PC + Acrylic-coating 4	High-Med	Non-PET option
3	PET + Fluorinated layer	Medium	PET with UV filter layer
13	PET + Fluorinated coating 2	Medium	PET with UV filter coating
4	PET + Acrylic-coating 3	Med-Low	PET with UV filter coating
6	PET + UV blocker 1 (high)	Med-Low	PET formulated with UV absorbers
8	PET + UV blocker 2 (high)	Med-Low	PET formulated with UV absorbers
9	PET + Acrylic-coating 1	Med-Low	PET with UV filter coating
11	PET + Acrylic-coating 2	Med-Low	PET with UV filter coating
12	PET + Fluorinated coating 1	Med-Low	PET with UV filter coating
5	PET + UV blocker 1 (low)	Low	PET formulated with UV absorbers
7	PET + UV blocker 2 (low)	Low	PET formulated with UV absorbers
2	PET #6 but no UV blocker	Lowest	Bare PET (Negative Control)
10	PET #9 but no Acrylic-coating	Lowest	Bare PET (Negative Control)

TABLE II
SAMPLE EXPOSURE CONDITIONS

Chamber	CAT (°C)	Chamber BPT (°C)	Chamber RH (%)	Sample Temperature (°C)	Sample RH (%)	UV Irradiance (W/m²/nm)
Ci5000-A3	65 °C	90 °C	20%	~70°C	16.2%	0.8
Ci4000 Modified	65 °C	90 °C	20%	50°C	39.6%	0.8
				80°C	10.8%	0.8
				70°C	16.2%	0.4
				70°C	16.2%	4
Ci5000-A5	85 °C	110 °C	20%	~90°C	16.2%	0.8

variability of the equivalence of accelerated stress tests. This then allows us to determine if a relevant amount of stress has been applied, to give some confidence that the materials showing very little degradation are likely to be adequate for the application. Here, we look at PV-relevant material degradation but focus on the appropriateness of the testing as opposed to the specifics of one film or material.

II. EXPERIMENTAL METHODS

Samples were obtained from various PV frontsheet and polymeric film manufacturers and exposed under different conditions in Atlas Ci5000s and in a modified Atlas Ci4000 Weather-Ometer as indicated in Table II. The Ci4000 used Al plates with circulated chilled water for cooling and one dedicated spot with a dummy sample equipped with a thermocouple for temperature control (see Fig. 1). The samples were pressed against the 152.4-mm × 152.4-mm Al plate with a spring-loaded silica glass plate in front to ensure good thermal contact [5]. The plates were able to be positioned at variable distances from the lamp to give irradiance levels between 0.4 and 4 W/m^2/nm. The xenon arc lamps used an Atlas CIRA-coated silica outer filter and a Right Light inner filter compliant with ASTM D7869 [6]. Separately, another set of samples was exposed in the dark to temperatures of 85 °C, 100 °C, 115 °C, and 150 °C.

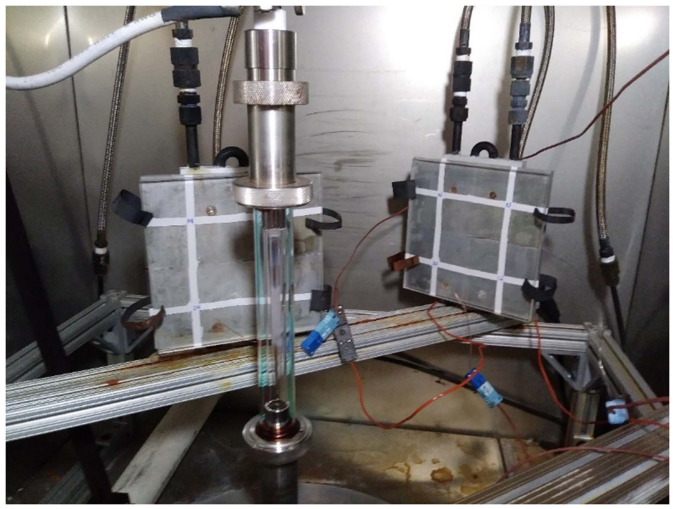

Fig. 1. Image of samples in the modified Atlas Ci4000 chamber.

The samples in the modified chamber were 38.1 mm × 38.1 mm and taped together in a grid using white polyvinyl fluoride-based tape (see Fig. 1). The 12.7-mm-thick Al plate temperatures are controlled using water cooling plates on the backside. The dummy sample used for temperature feedback control consists of a thermocouple embedded in a sample layered as poly(ethylene-co-tetrafluoroethylene) (PETFE)/EVA/PETFE. Samples are held in place using clips composed of spring steel pressing a 6.36 mm thick, 152.4-mm × 152.4-mm silica glass plate against the front surface. After each measurement cycle, the samples were rotated 90° to be placed in a new position. The irradiance level was determined as outlined by Kempe et al. [7] with additional adjustments accounting for a total of 8% loss from reflection at the two silica-to-air interfaces.

Prior experience with this equipment indicates that the temperature is controlled to better than ± 2 °C [5]. Because there are air gaps in the sample plane between the Al and silica plates, it is easily assumed that the samples will quickly reach equilibrium with respect to humidity in the chamber. Even if the plates were fully laminated together with EVA, the equilibration time would be measured in hundreds of hours and still not represent an important factor [8].

It is similarly possible that oxygen ingress could be limited. Oxygen is much less soluble than water, and in many cases, the consumption rate of oxygen is high enough to limit the extent of ingress. This could be an issue, but if it was, the degradation patterns would be locally affected by the contact quality to the glass or Al and would be likely to result in a mottled look which was not seen. While this is a potential effect, we see no evidence of oxygen being diffusion limited.

The samples in the Ci5000s were 76.2 mm × 63.5 mm, unbacked, and held in a 76.2-mm-wide sample holder. Using transparent test samples with embedded thermocouples, it was estimated that the temperature rise was about 5 °C above ambient with an estimated ± 3 °C variability in that value [5]. However, this assumption is only good until significant yellowing has occurred. Unfortunately, without extensive modification, it is

not possible to precisely know the exact temperature of every sample independently in this instrument.

The samples were evaluated at 0, 500, 1000, 1500, 2000, 3000, and 4000 h of exposure. The transmittance was measured from 200 to 1500 nm in 1-nm increments at all time intervals. From this, the solar photon quantum efficiency weighted transmittance (SPQEWT) was calculated as [9]

$$\text{SPQEWT} = \frac{\sum \lambda_i E(\lambda_i)\,\text{QE}(\lambda_i)\,\text{TRN}(\lambda_i)}{\sum \lambda_i E(\lambda_i)\,\text{QE}(\lambda_i)} \quad (1)$$

where λ_i is the wavelength [nm] for a particular measurement, $E(\lambda_i)$ is the energy in the solar spectrum at that wavelength, QE(λ_i) [%] is the quantum efficiency of the cell at that wavelength, and TRN(λ_i) [%] is the measured transmittance at that wavelength. For this experiment, a QE curve for a crystalline Si cell was used. The wavelength is included as a factor in this equation because the wavelength multiplied by the light energy intensity at that wavelength corresponds to the number of photons which corresponds to the energy-producing potential of the light in a PV module. This SPQEWT value correlates to the current generating potential of a cell with a frontsheet under a typical solar spectrum.

We also calculated the yellowness index (ASTM E313 [10]), average transmittance between 310 and 340 nm, and the UV cut-on wavelength where transmittance first reaches 10%. Spectra were collected in an Excel spreadsheet with macros used to calculate all the relevant parameters and the changes relative to initial measurements and then the final data were imported into JMP for analysis. Data were examined for consistency at each interval with many measurements being removed as the samples became embrittled, showed signs of thermal runaway, or otherwise degraded beyond what is relevant in a fielded module.

In this work, all error bars are an expression of one standard deviation.

III. Results

A. Thermal Aging

For the samples exposed in the dark, very little change was seen in transmittance except at temperatures of 150 °C (see Fig. 2). In the dark, a drop of up to 4% in transmittance was frequently seen in the first 500 h after which relatively little additional change was seen. Considering that it took temperatures above 100 °C to begin to see changes, it was concluded that degradation in the dark was either insignificant or beyond the ability of the experimental data to model accurately within the timeframe of the test. Furthermore, most of these samples experienced an initial drop which may or may not be just an initial "break-in" phase after which very little long-term change might be seen. With these considerations, it is not known if the degradation data are the result of relevant degradation modes.

Because degradation is occurring primarily at the highest temperature, we do not have appropriate data from which to determine thermal acceleration factors to do an extrapolation. The 85 °C data are not past the initial break-in, and the 100 °C and 115 °C data are too similar and would need to be run much longer to show significant degradation. At best we have two

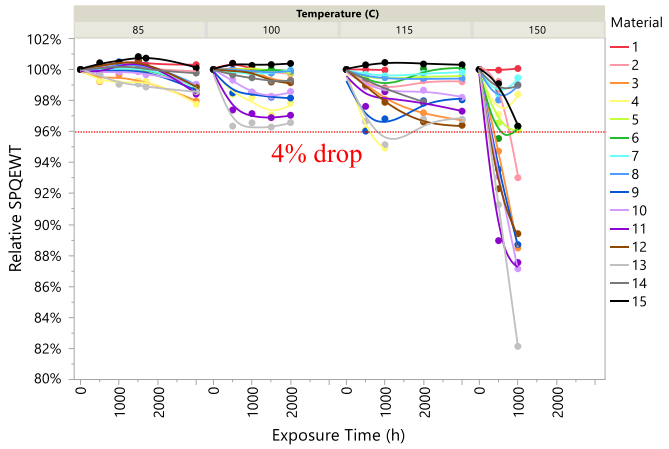

Fig. 2. Solar quantum efficiency weighted transmittance according to (1) for samples exposed in the dark to temperatures between 85 °C and 150 °C.

useful points at 115 °C and 150 °C and when extrapolated to the use temperature these degradation modes would be essentially nothing as the data at 85 °C have very little degradation. Therefore, the focus was put on the UV data understanding that temperature-only exposure does not seem to significantly degrade the optical properties of these materials at the temperatures generally seen under normal operating conditions. However, higher temperatures may be seen at hot spots under reverse bias shading.

B. UV Aging

1) Modeling Fit Equations: It is desirable to obtain degradation modeling parameters suitable for extrapolation from the lab to the use environment. The use of a single equation implies that one mechanism overwhelmingly dominates the degradation (R_D), which is rarely true, especially across a wide range of stress conditions. Usually, there are many competing reactions with different activation energies such that these single-mechanism types of models are at best true over a limited range of conditions. Therefore, minimizing the acceleration factors in an experiment is important for getting accurate extrapolation to the use conditions [3], [4]. This represents a significant assumption which is the primary reason why acceleration parameters are not obtained for all materials and measurements.

The modeling equation chosen is consistent with many other sources with a form of

$$R_D = R_o\,(\text{RH})^n G^P e^{-\frac{E_a}{RT}} \quad (2)$$

where RH [%] is the relative humidity, G [W/(m^2·nm)] is the irradiance at 340 nm, E_a [kJ/mol] is the Arrhenius activation energy, R is the universal gas constant, T [K] is temperature, P is the Schwarzchild constant [7], [11], [12], [13], [14], [15], n is a constant, and R_o is a prefactor to indicate the relative degradation of a particular mechanism. The units for R_o are what is necessary to produce R_D with units of *YI*/time, %/time, or whatever the units of a particular degradation mode are. Here, we are primarily concerned with values for n, p, and E_a; therefore, the particular units of R_o are unimportant for this analysis.

For temperature and irradiance, the Arrhenius form used here is very common and it requires atypically accurate and comprehensive data to be able to determine that a different form is more appropriate [1]. In contrast, this form for relative humidity dependence is one of many forms of equal probability of being correct [16]. Furthermore, as shown in [1] and [2], humidity may have no effect, a large positive effect, or a negative effect on degradation rates for paints and coatings. If the degradation process produces water as a byproduct in the rate-determining step, the presence of moisture can actually slow down degradation [17]. Using humidity as an accelerant for laboratory testing is risky because it will preferentially highlight mechanisms dependent on humidity leading to poor material/process comparison and poor extrapolation to the use environment. It is also common for the humidity dependence to be much more complicated (e.g., a Brunauer-Emmett-Teller (BET) isotherm) [18], [19] than shown in (2) making fitting it to a function more difficult [16]. Accelerated stress testing should be conducted at a humidity level that is representative of the use environment [16], [20]. Otherwise, one should determine the dependence on humidity, which is much more dependent on the specifics of the degradation mechanisms and not as amenable to generalizations.

The samples exposed in the same Atlas Ci4000 chamber with different temperatures were exposed to the same absolute humidity but to different relative humidity levels. Additionally, two Atlas Ci5000 chambers were used at different temperatures and humidity levels (see Table II). In theory, if the data have sufficient precision and the functional form is accurate, even the RH dependence n could potentially be determined despite RH not being systematically varied. The degradation data were analyzed in this way using the JMP software and (2) with a nonlinear fitting routine for each material to determine the optimal values for each of the degradation parameters. Unfortunately, we could not get good results for any of the degradation parameters for any of the materials. Because this method analyzes all six conditions at once, it is not easy to determine which of the experimental conditions or degradation parameters might be causing spurious results. Therefore, we limited the analysis to E_a and P only where we could look at small, systematically varied subsets of data in which abnormalities are easily seen. Specifically, this is where either only temperature or only irradiance intensity was varied between samples.

2) Change in Transmittance: For each measured parameter, the negative of its change relative to the initial value divided by the test time was used as a measure of the average degradation rate up to that point in time. The samples under the A3 condition [21] (70 °C sample temperature, 65 °C chamber temperature, 0.8 W/m^2/nm at 340 nm, and 16.8% RH sample humidity) were consistent outliers when plotted on an Arrhenius plot and were excluded from all the analyses. E_a was determined by plotting the natural logarithm of the degradation rate versus $1/T$ [1/K] for the three temperatures of 50 °C, 80 °C, and 90 °C, with E_a being equal to the slope of this line (determined as a least-squares fit of the natural logarithm) multiplied by the universal gas constant (see Fig. 3). Because negative degradation rates will not appear on this type of plot, samples for which a very small slope is determined simply have a degradation that is on the order of the measurement noise, which is biased by the removal of values with positive changes to produce this small slope. Because of this, data for all the different measurements which degraded less than 0.20%/1000 h were removed from the final analysis of the averages and standard deviations for the degradation modes. The concern is that the degradation was actually an average of around 0% but that the biased inclusion of only positive values would thus only produce random noise. For consistency, the determination of the 0.20%/1000 h degradation rate was made by interpolating the best-fit line at 70 °C using the values from the least-squares fit line.

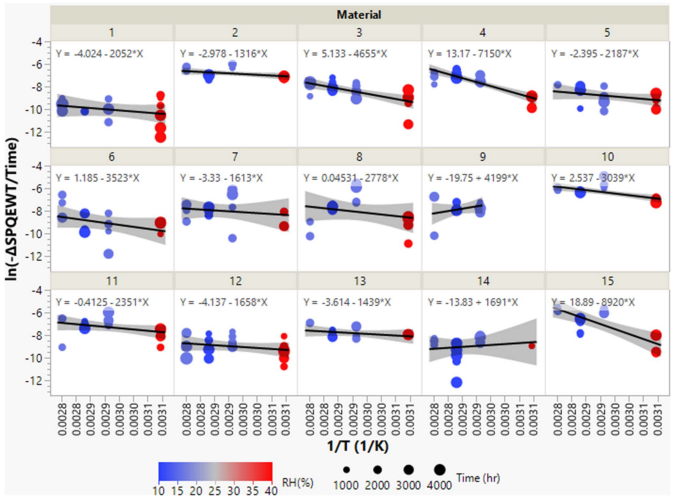

Fig. 3. Arrhenius plot to determine the activation energy for the loss of solar photon quantum efficiency weighted transmittance SPQEWT for 15 materials. The ordinate is the logarithm of the ratio of the total change over the total time or the logarithm of the average rate of change. The RH is 16.5%, 10.8%, or 39.8% at temperatures of 90 °C, 80 °C, and 50 °C, respectively. This plot excludes measurements under the A3 condition. Materials #1, #6, #8, #9, #12, and #14 were excluded from the determination of $E_{a\,T} = 30.7 \pm 23.5$ kJ/mol. Variability is for one standard deviation.

In Fig. 3 the SPQEWT transmittance is plotted with the RH indicated by different colors and the total exposure time by the size of the marker. Here, we see no systematic dependence on humidity or on exposure time that is above statistical background levels. However, the humidity did vary systematically with temperature making it possible that the humidity dependence is buried in the results that would have led to a reduction in degradation rates at high temperatures and a reduction in predicted activation energy. For context, the partial pressure of water in the air increases with an activation energy of about 40 kJ/mol. If moisture had a linear effect on degradation, we would have seen a reduction in the slope between the 50 °C and 80 °C data points where the humidity changes from 39.6% to 10.8% causing a factor of ~4 × reduction in degradation rate. But the 90 °C data have an RH value of 16.5% which would create an increase in slope between the 80 °C and 90 °C points of a factor of 16.5/10.8 = 1.52 ×. In Fig. 3, this would look like a concave up curvature to the lines with a change in slope on the order of twice the typical slope seen. Therefore, it is reasonable to assume that for at least most of these materials, the humidity

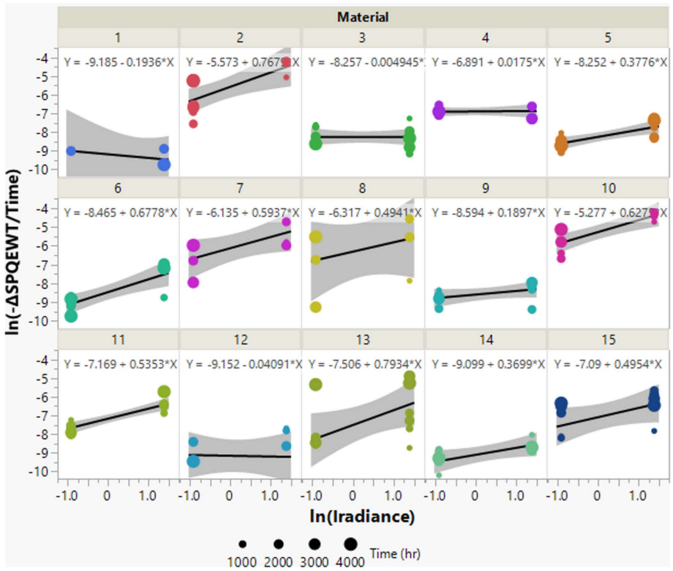

Fig. 4. Plots used to determine the dependence of P for the loss of SPQEWT. The ordinate is the logarithm of the ratio of the total change over the total time or the logarithm of the average rate of change. The RH is 16.2% for all three irradiance levels. Materials for #1, #3, #4, and #12 were excluded from the determination of $P_T = 0.53 \pm 0.17$. Variability is for one standard deviation.

dependence is of less importance than a first-order relationship to relative humidity.

There were several materials that were excluded from the computation of degradation mode averages. Sample #9 did not produce reasonably measurable degradation for the 90 °C exposure and hence did not produce reliable data. Similarly, #1 had a lot of noise at the 90 °C point and did not meet the minimum degradation rate criteria. Also, #6, #8, #12, and #14 also had low ($<$ 0.20%/1000 h) degradation rates and were excluded from the calculations of the averages. Because degradation modes are rarely the result of a single mechanism, they only work well with an Arrhenius analysis if one of the mechanisms dominates all the others as the rate-determining step. This is also part of the explanation for why in this, and the remaining analyses, a lot of data were not useable. For transmittance, the remaining nine samples, as a set, see an average activation of 31 $\pm$ 24 kJ/mol for the loss of SPQEWT (see Fig. 3). In this and all similar subsequent calculations, the variability was calculated as arising from both the individual measurement uncertainty and the total variability between all the samples.

Similarly, the degradation dependence on irradiance intensity P can be directly determined as the slope of the logarithm of the degradation rate versus ln(G) at 340 nm in units of W/m^2/nm (see Fig. 4). For this, we have exposures at 70 °C, 16.2% RH with 0.4, 0.8, and 4.0 W/m^2/nm at 340-nm irradiance levels. For the estimation of P for this and the other degradation modes, we use the data at the A3 condition because using only two test conditions is more of a concern than using questionable data. However, the exposure will still span a factor of 10 for light intensity providing a reasonably expansive distribution of data for fitting the curves. For low rates of degradation, random noise leads to slopes with positive changes in SPQEWT, which cannot be plotted on a logarithmic axis which, like what was done for the activation energy, creates an inherent systematic bias justifying the removal of data for which $P < 0.1$ (excluded materials #1, #3, #4, and #12).

Like the Arrhenius analysis, the multitude of mechanisms in these degradation processes combined with the empirical nature of the power law relationship is certainly a large part of the explanation for why so many materials did not fit well to produce a value for P. Only a detailed chemical/mechanistic analysis could accomplish this which is an entire research project in itself for every chemical reaction.

With the remaining 11 materials, it was found that as a set $P = 0.53 \pm 0.17$ for loss of SPQEWT. Here it is recognized that the elimination of low values ($<$0.1) of P can introduce a systematic bias, but in these cases, it is also likely that the degradation rate is either too slow to be measured or that the degradation is not dependent on light. In this context, this analysis should be interpreted as being applicable only to processes that are significantly dependent on light intensity.

In the next sections, the degradation parameters E_a and P were similarly determined for *YI* changes and loss of UV absorption. For these degradation modes, samples with $P < 0.1$ or values for $R_D < 0.20\%$/1000 h at 70 °C were excluded because these samples essentially did not degrade with respect to this parameter making these low activation energies likely to be just a function of the experimental noise and consequent bias.

3) Yellowness Index Changes: For *YI* changes, only three of the materials (#1, #12, and #14) degraded too little to be suitable for the determination of parameters. The activation energy was similar to the SPQEWT with values in the range of $E_{aYI} = 40.4 \pm 22.5$ kJ/mol (see Fig. 5). The irradiance was also highly sublinear with $P_{YI} = 0.50 \pm 0.25$ (see Fig. 6).

4) UV Transmittance Changes: The change in UV transmittance, herein defined as the average transmittance between 310 and 340 nm, can be thought of as a measurement of the amount of UV absorber in the film. However, other components can degrade in such a way as to absorb in this range decreasing the transmittance, or the UV absorber can degrade to become more transmitting in this range. The production of UV chromophores is more probable, but any combination of production or destruction of absorption can occur simultaneously. Furthermore, some of the materials are just fluoropolymer films with no moieties to absorb UV light or to degrade into something that will degrade to absorb UV light. Because of this, UV transmittance is not as useful for producing modeling parameters.

Once samples are eliminated because the degradation rate is too low or because the slope of the curve is too low (R_D $<$ 0.20%/1000 h at 70 °C) to be definitively above experimental noise levels, only materials #4, #5, #6, and #13 were useful resulting in $E_{aUV} = 53.2 \pm 16.6$ kJ/mol (see Fig. 7). Materials #14 and #15 seem to have a degradation that is resulting in the formation of chromophores. But for #14, the formation rate is low as is expected for a fluoropolymer. For both #14 and #15, there is just one, potentially spurious data point at a high temperature which is causing the line of fit to have the slope it does. With these considerations, we did not include these materials which may be producing UV chromophores.

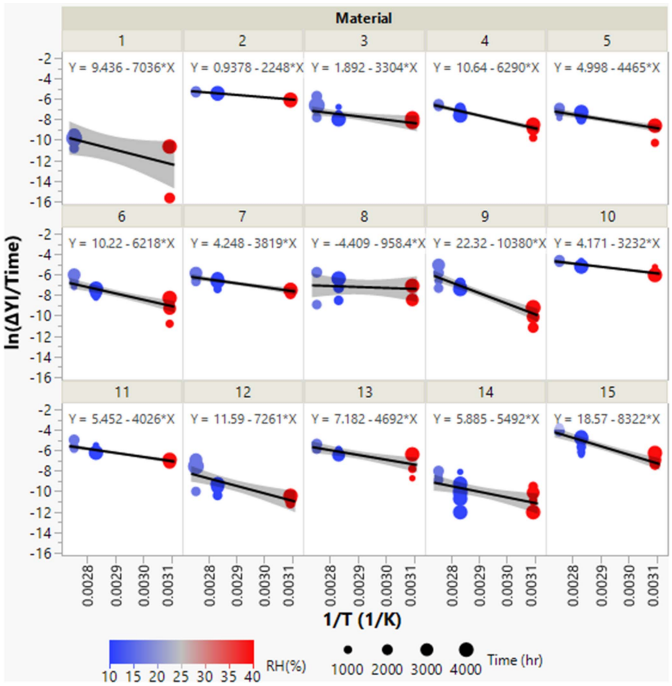

Fig. 5. Arrhenius plot to determine the activation energy for the change in yellowness index. The ordinate is the logarithm of the ratio of the total change over the total time or the logarithm of the average rate of change. The RH is at 10.8%, 16.5%, or 39.8% at temperatures of 90 °C, 80 °C, and 50 °C, respectively. Materials #1, #12, and #14 were excluded from the determination of $E_{a\,YI} = 40.4 \pm 22.5$ kJ/mol. Variability is for one standard deviation.

Even though material #13 did not degrade much, it did display an interesting degradation profile in the UV. When the transmittance is plotted logarithmically (see Fig. 9), the spacings for the absorption are approximately evenly spaced. Inspection of Figs. 7 and 8 show that the earlier times (smaller dots) show a systematically lower degradation rate as would be expected. The trend is more pronounced at the lower irradiance levels with the data set at 80 °C in Fig. 7 being the clearest example. The reduced consistency at 4 W/m^2/nm was due to most of the UV absorber being consumed and the transmittance reaching a maximum of around 6% in the UV range. This indicates that the UV absorber is degrading into a compound that is much less effective at UV absorption. The reduced consistency at 0.4 W/m^2/nm or at 50 °C is due to the degradation being much lower and consequently more subject to measurement precision issues.

For the irradiance intensity materials #5, #6, #13, and #15 were useful, having a sufficiently large degradation and P>0.1, resulting in $P_{\mathrm{UV}} = 0.45 \pm 0.32$ (see Fig. 8).

The logarithmic increase in transmittance can be understood as a constant loss of UV absorber where the total transmittance is governed by the Beer–Lambert law as

$$I_{UV} = I_o\, e^{-\mu C l} \tag{3}$$

where I_o is the incident light, I_{UV} is the transmitted light intensity, μ is the Napierian attenuation coefficient indicating the absorption per unit concentration and length [cm^2/g], C is the concentration of absorbing species, and l is the thickness of the absorbing medium. The transmittance in the UV, i.e., T_{UV},

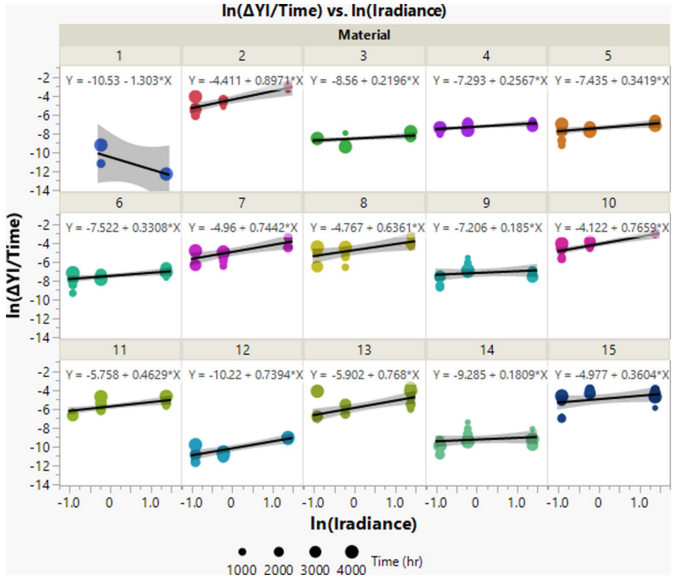

Fig. 6. Plots used to determine the dependence of P for YI changes. The ordinate is the logarithm of the ratio of the total change over the total time or the logarithm of the average rate of change. The RH is 16.2% for all three irradiance levels. Materials #1, #12, and #14 were excluded from the determination of $P_{YI} = 0.50 \pm 0.25$. Variability is for one standard deviation.

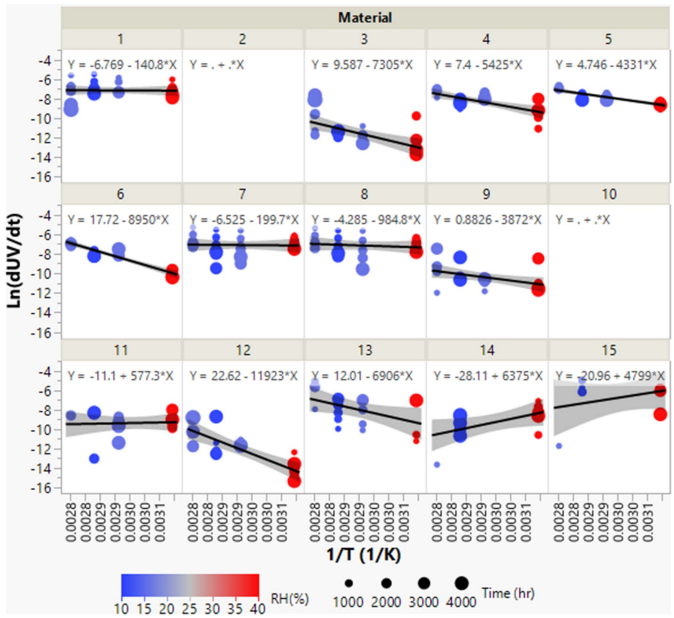

Fig. 7. Arrhenius plot to determine the activation energy for the change in UV transmittance. The ordinate is the logarithm of the ratio of the total change over the total time or the logarithm of the average rate of change. The RH is at 10.8%, 16.5%, or 39.8% at temperatures of 90 °C, 80 °C, and 50 °C, respectively. Only materials #4, #5, #6, and #13 were useful for the determination of $E_{a\,UV} = 53.2 \pm 16.6$ kJ/mol. Materials #2 and #10 do not have data because all the slopes had the opposite sign and will not plot on the same logarithmic axis. Variability is for one standard deviation.

is the ratio of I_{UV}/I_o and the rate of change of the logarithm of T_{UV} can be found from the derivative of (3) as

$$\frac{d\left[\ln\left(\frac{I_{\mathrm{UV}}}{I_o}\right)\right]}{dt} = \frac{d\left[\ln\left(T_{\mathrm{UV}}\right)\right]}{dt} = -\mu l \frac{dC}{dt}. \tag{4}$$

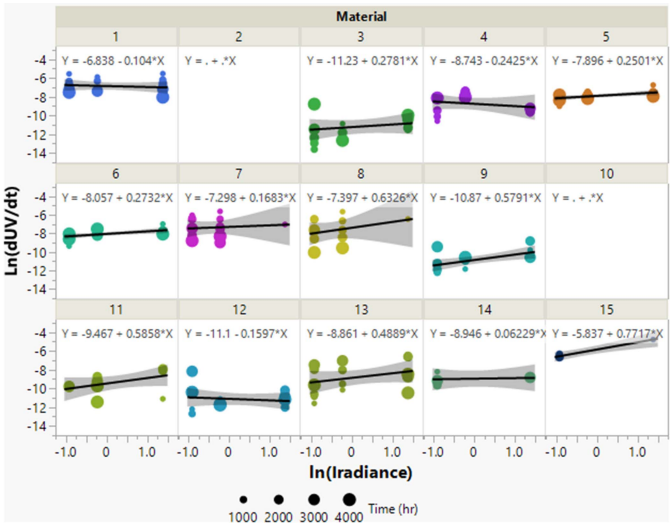

Fig. 8. Plots used to determine the dependence of P for UV transmittance change. The ordinate is the logarithm of the ratio of the total change over the total time, or the logarithm of the average rate of change. The RH is 16.2 for all three irradiance levels. Only data for #5, #6, #13 and #15 were used for the determination of $P_{\mathrm{UV}} = 0.45 \pm 0.24$. Variability is for one standard deviation.

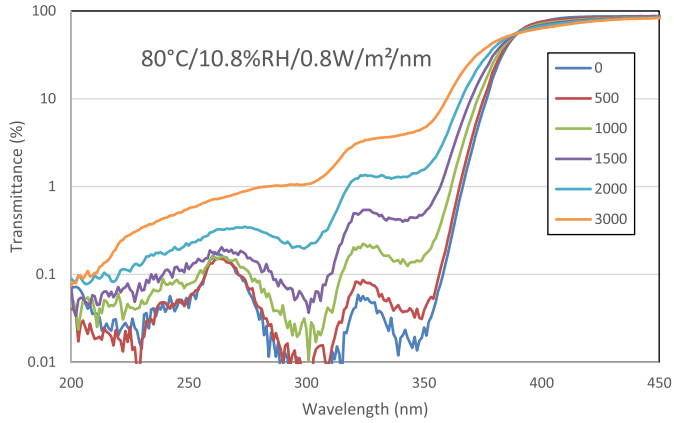

Fig. 9. Material #13, a PET with a UV filtering coating and a fluoropolymer layer, during exposure to 80 °C, 10.8% RH, and 0.8 W/m^2/nm at 340 nm. $Ea = 33.9 \pm 7.1$ kJ/mol, $P = 0.33 \pm 0.07$. Uncertainty is for one standard deviation using data with significant changes but less than 1% loss (e.g., 500 h to 2000 h above).

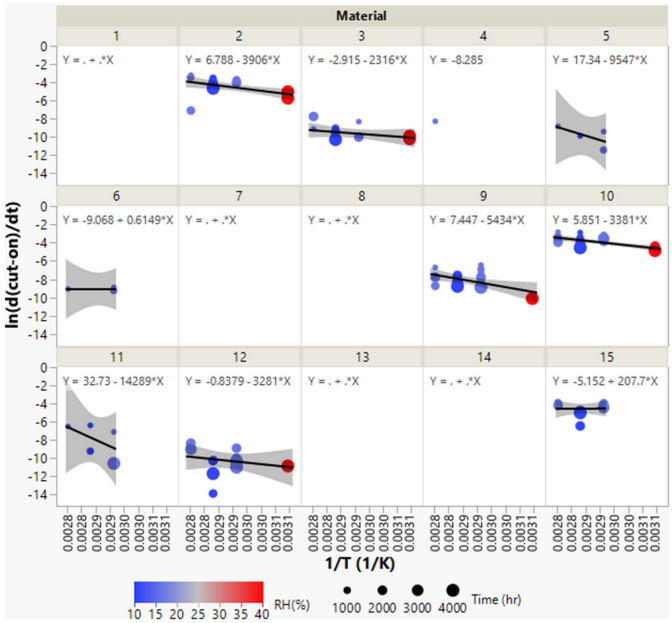

Fig. 10. Arrhenius plot to determine the activation energy for the change UV cut-on defined as the wavelength where the transmittance first reaches 10%. The ordinate is the logarithm of the ratio of the total change over the total time, or the logarithm of the average rate of change. The RH is at 10.8%, 16.5%, or 39.8% at temperatures of 90 °C, 80 °C, and 50 °C, respectively. Only materials #2, #9, and #10 were useful for the determination of $E_{a\,UV} = 35 \pm 8.9$ kJ/mol. Many materials do not show data on this plot because all the data points had the opposite sign. Variability is for one standard deviation.

For material #13, there is a limited amount of UV absorber which decomposes to produce something that is much less UV absorbing. Furthermore, this degradation rate is relatively constant which can be understood as dependent on the incident light which is absorbed almost completely absorbed (90%–99.9%) creating a fixed production rate of degradation byproducts. When most of the UV absorber is converted to the byproduct about 6% of the light is transmitted as opposed to less than about 0.03%. Using these numbers in (3), the ratio of C for the original UV absorber to C for the byproduct is greater than 5.3 indicating that less than 20% of the UV absorber is still active. While the degradation rate does appear to be nearly constant, the UV-induced mechanism assumption does not exactly predict a constant degradation. With 80% of the UV absorber being degraded, the remaining 20% must still be absorbing enough of the UV light and degrading which indicates that most of the degradation is occurring in the top $\sim$<20% of the film or we would have seen more of a change from the linear loss mechanism in Fig. 9. The UV absorber must be heavily depleted on the UV facing side as the degradation rate is dependent on the amount of UV light present, otherwise we would see a decreasing degradation rate.

In Figs. 7 and 8, materials #1 and #8 have the opposite trend of a decreasing degradation rate in time, but of a much smaller magnitude and with no dependence (or at least negligible amounts) on the temperature and light intensity. Material #1 is a fluoropolymer PETFE which cannot produce UV chromophores. This change in UV transmittance can be explained by changes in the roughness or other aging processes that are more mechanical in nature. Surface roughness or contamination would cause changes of greater magnitude in the UV portion of the spectrum.

5) UV Cut-On Changes: The UV cut-on is defined here as the wavelength where the transmittance first reaches 10%. It is a good metric for changes in the presence and chemical composition of UV absorbers. Just like the UV transmittance discussed in the previous section, there are many ways for UV absorbers to degrade making the attainment of useful modeling parameters difficult. Furthermore, some of these materials did not contain UV absorbers so that a UV cut-on wavelength could not be computed. For the thermal activation energy, only three samples, #2, #9, and #10, were used to give $E_a = 35.3 \pm 9.0$ kJ/mol (see Fig. 10). For light intensity, samples #2, #10, #13, and #15 were used to give $P = 0.37 \pm 0.26$. Fig. 11.

TABLE III
SUMMARY OF DEGRADATION PARAMETERS UNCERTAINTY IS FOR ONE STANDARD DEVIATION

Measurement	*Ea* (kJ/mol)	# Samples	*P*	# Samples	Correlation Coefficient	# Samples
UV Cut-on	**35.3±8.9**	**3**	**0.37±0.26**	**4**	**NA**	**2**
UV Transmittance (310 nm to 350 nm)	**53.2±16.6**	**4**	**0.45±0.24**	**4**	**0.093**	**3**
Yellowness Index	**40.4±22.5**	**12**	**0.50±0.25**	**12**	**-0.637**	**11**
Solar Photon Quantum Efficiency Weighted Transmittance (SPQEWT)	**30.7±23.5**	**9**	**0.53±0.17**	**11**	**-0.646**	**6**
Average	**38.7±21.7**	**28**	**0.49±0.22**	**32**	**-0.606**	**22**
Fischer and Ketola [1, 2]	**~36±18**		**0.64±0.20**			

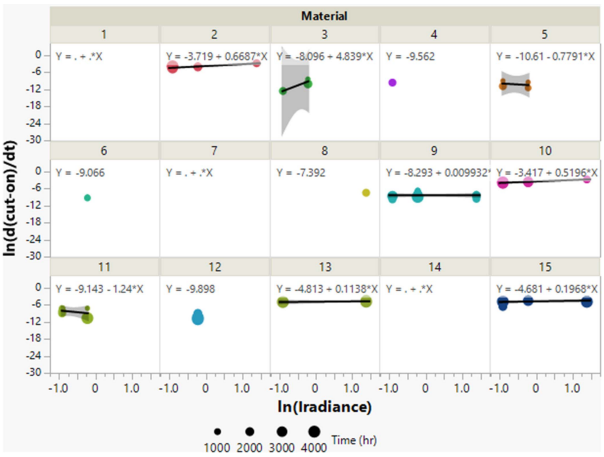

Fig. 11. Plots used to determine the dependence of P for the change in UV cut-on defined as the wavelength where the transmittance first reaches 10%. The ordinate is the logarithm of the ratio of the total change over the total time, or the logarithm of the average rate of change. The RH is 16.2 for all three irradiance levels. Only data for materials #2, #10, #13, and #15 were useful for the determination of $P_{\mathrm{UV}} = 0.37 \pm 0.26$. Materials #1, #4, #8, and #14 do not show data because all the points had the opposite sign. Variability is for one standard deviation.

6) Summary of Acceleration Parameters: The summary for all these measurements is given in Table III. Here one can see that for some of the parameters, very few data sets produced useable values. The global averages and standard deviations were obtained by considering all the data points individually as one set of data. With this compiled set of data, there were 22 material/measurement combinations where both the activation energy and irradiance intensity factor were useable. From this, we obtained a correlation coefficient of -0.606. This is a medium-strength correlation indicating that for highly thermally activated processes there was less dependence on irradiance and vice versa. This is consistent with the understanding that degradation processes that are promulgated by photons tend to be weakly activated [1], [2] and that thermal-only activation tends to be more highly activated [22].

IV. DISCUSSION

In this experiment, we are not trying to evaluate the specific sources of the degradation from a mechanistic standpoint for a service life prediction and have instead only focused on the degradation modes. A mechanistic understanding could entail an entire research project for each material and/or for each mechanism of each material. This is beyond the scope of this project. Ultimately, we wanted to know which of these materials is possibly adequate for a PV application and to know what is the rough timescale equivalence of the testing protocols we have utilized. Not knowing the exact mechanism causing failure in a specific film is not important when trying to determine the range of failure acceleration factors. What is important is that the modes and materials are relevant and that the stress levels are not so high that the degradation might not be relevant. It should be noted that while *YI* is not directly relevant to PV performance, it does represent absorption processes that occur in the blue region of the spectrum and is thus correlated with relevant degradation parameters.

A detailed mechanistic understanding would be specific to a particular frontsheet and thus primarily of interest to the final frontsheet producer. We have some of this detailed information, but here we are trying to evaluate the more generally applicable information to use it to evaluate the testing strategy for application to the industry as a whole as opposed to specific materials.

In a detailed study of degradation parameters relative to durability testing of 50 different paints and coatings, Fischer and Ketola [1], [2] found similar parameters for typical degradation kinetics with variabilities of the same order of magnitude. Instead of looking at RH, they used time of wetness (TOW) which is the time a sample sees a humidity above 85 °C outdoors or the time in the chamber where it is being sprayed. They found that the average effect of TOW was far less than the variability in the effect of humidity. Without knowing the specifics of a test, the effect of increased humidity is just as likely to slow down degradation as to speed it up, making it not useful for accelerated stress test design.

For temperature, they found that the Van't Hoff equation fits the data more often than did the Arrhenius equation and provided Van't Hoff parameters. However, the forms of these equations are similar enough that one can calculate an effective Arrhenius activation energy for the Fischer et al. work as shown in Table III. Here, we see good agreement indicating a low thermal activation for UV degradation as seen by Fischer and Ketola.

Finally, both this work and that of Fischer show a highly sublinear effect of light intensity on degradation with a similar variability across the set of materials. This has important implications for test design because exposing materials to the same dose in an accelerated manner as would be seen in use would be highly underexposing a material if other factors are not accelerated.

Determining a typical degradation parameter range is extremely useful when one wants to get an understanding of the general approximate equivalence of an accelerated stress test. This question gets asked frequently in the standards community when we contemplate extending the duration or severity of a test and is particularly important in the context of expensive UV testing.

The sample set average activation energy and Schwartzchild constant along with the associated uncertainties and correlation coefficients from Table III were used in a Monte Carlo simulation. This was accomplished using a Microsoft Visual Basic macro in an Excel spreadsheet. First, a list of 20 000 random values for the activation energy was generated with a normal distribution, then a list of 20 000 corresponding values for P was generated accounting for the corresponding value of Ea to result in the correct correlation coefficient. For the simulation run used here, this produced $E_a = 38.5 \pm 21.5$, $P = 0.49 \pm 0.22$, and Cor $= -0.606$. Typical Model Year data from Riyadh Saudi Arabia was obtained from the International Weather for Energy Calculations Database [23]. Then, Python code for calculating the irradiance on the system was downloaded from the PVlib library on GitHub.com and used with the King model [24] for a rack-mounted polymer-back PV module to produce a series in 1-h time increments of temperature and irradiance data. Because the IWEC database only provides an average total irradiance value, as opposed to it being spectrally resolved in the UV region, we assumed that for every 1000 W of plane of array irradiance that 0.5018 W/m^2/nm irradiance existed at 340 nm [25], [26] for comparison with a UV chamber using a high fidelity xenon-arc lamp [27]. Then, with this series of acceleration factors, (2) is used to calculate the equivalent time for all 20 000 iterations producing the histograms in Fig. 12.

Riyadh, Saudi Arabia was chosen as an example of one of the hottest environments. This is for a south-facing fixed latitude tilt insulated back system. It is possible to get even more severe climates by not having the system pointing due south and using a more summer-optimized tilt [28], but this is only expected to be marginally more severe. However, considering that the purpose of this work is to develop lightweight PV panels to be directly applied to a roof surface, which is likely to be insulated, using higher-temperature model environments is appropriate.

The Monte Carlo simulation in Fig. 12(a) relates to a 4000 h exposure of the most extreme condition of this test. It is only

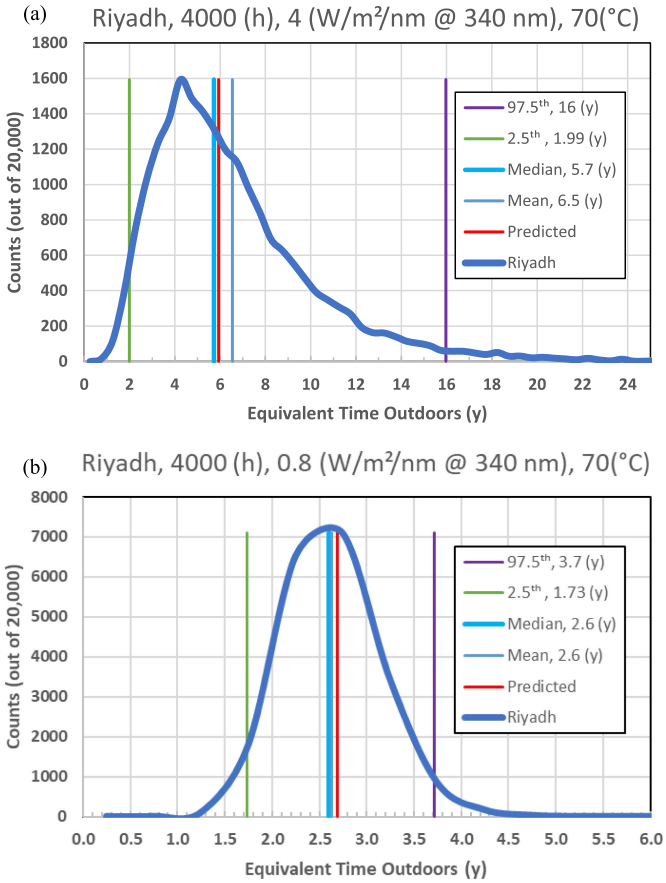

Fig. 12. Histogram of predicted Riyadh, Saudi Arabia lifetime equivalent of 4000 h chamber exposure from Monte Carlo Simulation using 20 000 iterations. Showing the 97.5th percentile, the 2.5th percentile, Median, Mean, and the value predicted from a calculation using the average values for $E_a = 38.7 \pm 21.7$ kJ/mol, $P = 0.49 \pm 0.22$, and Corr $= -0.606$. The thermal model is for insulated back modules at fixed latitude tilt. Counts are determined using 0.5 y bins. (a) Highest light intensity exposure. (b) Condition A3.

equivalent to about 5.7 years and the more commonly used A3 condition was only equal to about 2.6 years on average [see Fig. 12(b)]. These lengths of time are a good start, but not enough to give confidence in a lifetime of 25 years. However, we do not necessarily need a lifetime prediction. What this is demonstrating is that the exposure used will capture infantile failure. If we then select materials for which there is essentially no degradation in the test, then it is reasonable to assume that if a failure does begin to happen after around 5.7 years that it will be slower and that the loss in performance after 25 years is not expected to be too great. Several of the materials showed degradation rates low enough to be just above background noise levels and were neglected from this analysis. Even though some of these did still show some indication of a temperature or irradiance dependence to indicate that the degradation may be above noise levels, it is still likely to be of negligible extent by an end of life.

Python code was also utilized to assess the equivalent time for 10,041 sites worldwide [29]. Here we just used the average values of $E_a = 38.7$ kJ/mol and $P = 0.49$ in the calculation and

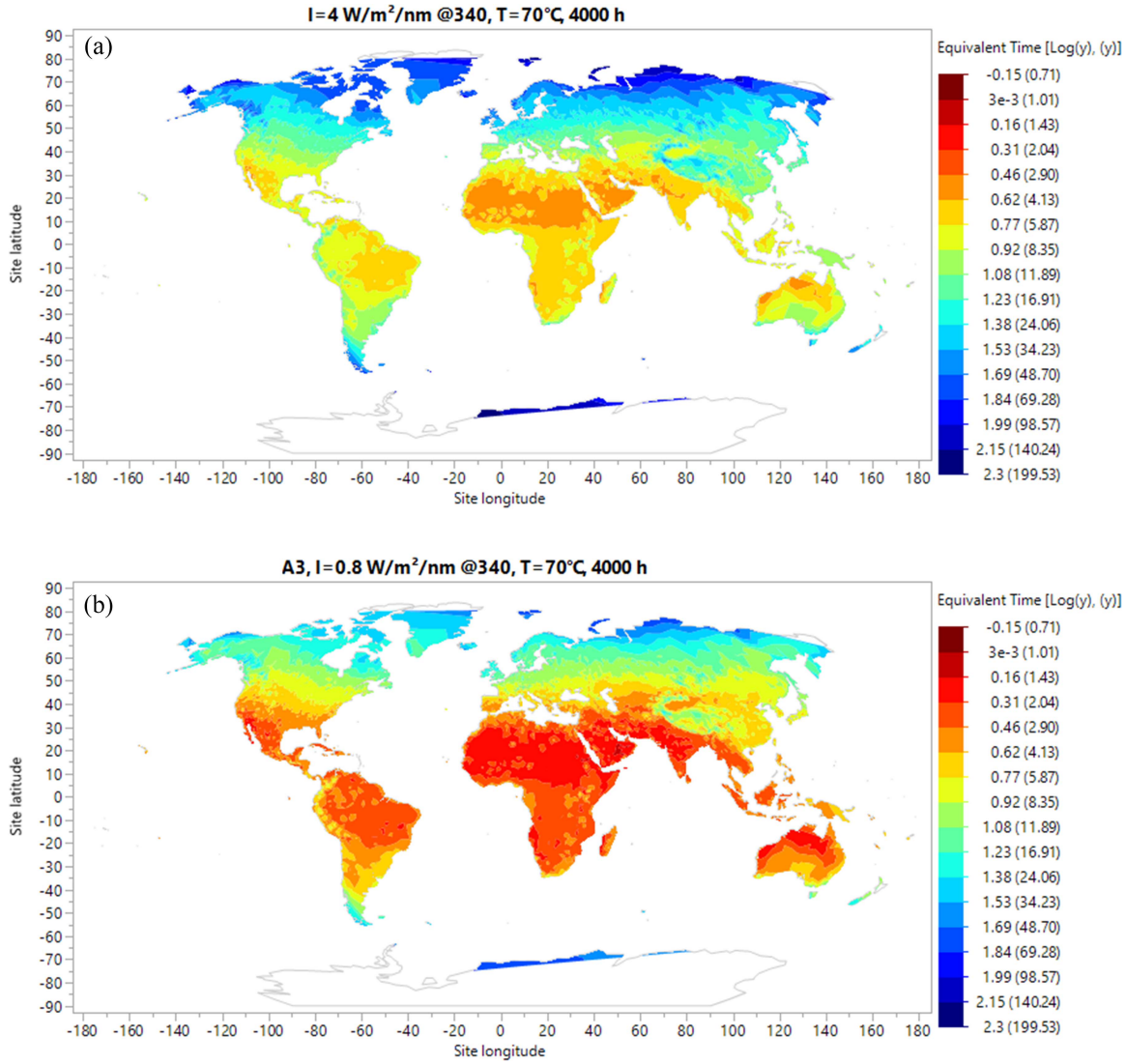

Fig. 13. Map of mean test equivalent lifetime (ignoring variability between mechanisms) with $E_a = 38.7$ kJ/mol and $X = 0.49$. The thermal model is for insulated back modules at fixed latitude tilt. Colors are the log10 of the time and the time indicated in parentheses. Equivalent time is calculated for a chamber exposure time of 4000 h. (a) Highest light intensity exposure. (b) Condition A3.

compute the equivalent outdoor time to 4000 h of chamber exposure (see Fig. 13). With this, one can see that only the extreme equatorial deserts are severely damaging or have a short equivalent exposure time. For most of the northern climates, where applying PV to an insulated roof is not a serious thermal concern, the equivalent time of the more severe test is between 10 and 25 years. But for the A3 condition, this is only equivalent to 2.5 to 15 years which might not be sufficiently long to have confidence in the performance. With this, we can see that for a large majority of nonequatorial sites, a sample showing little to no degradation in tests is reasonably likely to be sufficiently durable.

V. Conclusion

In these tests, we have not delved into the specific degradation mechanisms but instead focused on degradation modes to get a more generalized understanding of the acceleration factors for frontsheets. This general understanding of degradation kinetics is important if one wants to develop standardized tests that are suitable for a variety of materials without knowing ahead of time what the degradation acceleration factors are [30]. This understanding will better enable tests to be designed with reasonable acceleration factors and with an appropriate balance of these factors. Doing this can dramatically improve the interpretation of the results enabling reasonable confidence in producing an accurate rank ordering of different materials. It is essential in test designs that one balance thermal, UV, and hydrolytic stress factors to have the same equivalence to avoid biasing the test results.

The average acceleration factors found here are consistent with that from other sources in that the UV degradation process is only weakly thermally activated $E_a = 38.7 \pm 21.7$ kJ/mol, humidity has an uncertain effect on degradation (R_D), and the UV dose (Irr) is highly sublinear $P = 0.49 \pm 0.22$. Also of interest is the fact that materials that are highly thermally activated tended to be less affected by higher intensity irradiation with a moderate correlation of Corr $= -0.606$.

The frontsheets investigated here are intended to be used in systems installed directly onto roofing materials which in some cases will be insulated. This configuration is known to produce the highest normal operating temperatures. The test conditions used here are roughly equivalent to a few years. However, if they are used to screen and select materials which show very little or no degradation then one can reasonably expect little to no degradation for the first few years which are the most financially important time of a PV project's life. Then, even in the unlikely event that noticeable degradation begins to happen it is unlikely to be of sufficient magnitude to financially ruin a project. Thus, with a strong screening equal to several years outdoors, materials which do not show significant degradation there is a reasonable probability that no serious degradation will be seen for a 25-y lifetime of the modules with respect to frontsheet degradation. But there is still the probability that the degradation is highly nonlinear and could occur all at once later in its service life. So, as with any accelerated stress test, especially at high acceleration rates, there would still be some probability of a false positive conclusion [3]. Once this first level of screening is done, more and longer-term exposure should be conducted to increase confidence levels in long-term performance. The understanding of typical acceleration factors given here can help in the design of such a test because similarly to Fig. 12, the probable range of equivalence time for a test can be estimated.

References

[1] R. M. Fischer and W. D. Ketola, "Error analyses and associated risk for accelerated weathering results," in *Proc. 3rd Int. Serv. Life Symp.*, 2004.

[2] J. W. Martin, R. A. Ryntz, and R. A. Dickie, *Service Life Prediction: Challenging the Status Quo*. Philadelphia, PA, USA: Fed. Soc. Coatings Technol., 2005, pp. 79–92.

[3] W. Q. Meeker and L. A. Escobar, "Pitfalls of accelerated testing," *IEEE Trans. Rel.*, vol. 47, no. 2, pp. 114–118, Jun. 1998, doi: 10.1109/24.722271.

[4] T. J. McMahon, G. J. Jorgensen, R. L. Hulstrom, D. L. King, and M. A. Quintana, "Module 30 year life: What does it mean and is it predictable-achievable?," Sandia National Lab., Albuquerque, NM, USA, Rep. SAND2000-0912C, 2000. [Online]. Available: https://www.osti.gov/biblio/755637

[5] M. D. Kempe et al., "Evaluation of the durability of flexible barrier materials," in *Proc. IEEE 42nd Photovolt. Spec. Conf.*, 2015, pp. 1–6, doi: 10.1109/PVSC.2015.7355605.

[6] *Standard Practice for Xenon Arc Exposure Test With Enhanced Light and Water Exposure for Transportation Coatings*, ASTM D7869-13, 2013.

[7] M. D. Kempe, M. Kilkenny, T. J. Moricone, and J. Z. Zhang, "Accelerated stress testing of hydrocarbon-based encapsulants for medium-concentration CPV applications," in *Proc. IEEE 34th Photovolt. Spec. Conf.*, 2009, pp. 001826–001831, doi: 10.1109/pvsc.2009.5411508.

[8] M. D. Kempe, A. A. Dameron, and M. O. Reese, "Evaluation of moisture ingress from the perimeter of photovoltaic modules," *Prog. Photovolt., Res. Appl.*, vol. 22, pp. 1159–1171, Nov. 2014, doi: 10.1002/pip.2374.

[9] *Measurement Procedures for Materials Used in Photovoltaic Modules - Part 1-7: Encapsulants - Test Procedure of Optical Durability*, IEC 62788-1-7:2020, 2020.

[10] *Standard Practice for Calculating Yellowness and Whiteness Indices From Instrumentally Measured Color Coordinates*, ASTM E313-05, 2005.

[11] K. P. Scott and H. K. Hardcastle Iii, "A new approach to characterizing weathering reciprocity in xenon arc weathering devices," in *Proc. Serv. Life Prediction Polym. Mater.*, 2009, pp. 83–92.

[12] D. Miller, M. D. Kempe, C. E. Kennedy, and S. Kurtz, "Analysis of transmitted optical spectrum enabling accelerated testing of CPV designs," *Proc. SPIE*, vol. 7407, 2009, Art. no. 74070G.

[13] J. W. Martin, J. W. Chin, and T. Nguyen, "Reciprocity law experiments in polymeric photodegradation: A critical review," *Prog. Org. Coatings*, vol. 47, no. 3, pp. 292–311, 2003, doi: 10.1016/j.porgcoat.2003.08.002.

[14] J. E. Pickett, D. A. Gibson, and M. M. Gardner, "Effects of irradiation conditions on the weathering of engineering thermoplastics," *Polym. Degradation Stability*, vol. 93, no. 8, pp. 1597–1606, 2008, doi: 10.1016/j.polymdegradstab.2008.02.009.

[15] G. Jorgensen et al., "Use of uniformly distributed concentrated sunlight for highly accelerated testing of coatings," National Renewable Energy Lab., Golden, CO, USA, Rep. NREL/CP-520-28579. [Online]. Available: https://www.osti.gov/biblio/772423, doi: 10.1021/bk-2002-0805.ch006.

[16] M. D. Kempe and J. H. Wohlgemuth, "Evaluation of temperature and humidity on PV module component degradation," in *Proc. IEEE 39th Photovolt. Spec. Conf.*, 2013, pp. 0120–0125.

[17] X. Gu et al., "Linking accelerated laboratory test with outdoor performance results for a model epoxy coating system," in *Service Life Prediction of Polymeric Materials*, J. W. Martin, R. A. Ryntz, J. Chin, and R. A. Dickie, Eds. Berlin, Germany: Springer, 2009, pp. 3–28.

[18] D. J. Coyle, "Life prediction for CIGS solar modules part 1: Modeling moisture ingress and degradation," *Prog. Photovolt., Res. Appl.*, vol. 21, pp. 156–172, Mar. 2013, doi: 10.1002/pip.1172.

[19] D. J. Coyle et al., "Life prediction for CIGS solar modules Part 2: Degradation kinetics, accelerated testing, and encapsulant effects," *Prog. Photovolt., Res. Appl.*, vol. 21, pp. 173–186, Mar. 2013, doi: 10.1002/pip.1171.

[20] J. H. Wohlgemuth and M. Kempe, "Equating damp heat testing with field failures of PV modules," in *Proc. IEEE 39th Photovolt. Spec. Conf.*, 2013, pp. 0126–0131.

[21] *Measurement Procedures for Materials Used in Photovoltaic Modules - Part 7-2: Environmental Exposures - Accelerated Weathering Tests of Polymeric Materials*, IEC TS 62788-7-2:2017, 2017.

[22] R. R. Dixon, "Thermal aging predictions from an Arrhenus plot with only one data point," *IEEE Trans. Electr. Insul.*, vol. EI-15, no. 4, pp. 331–334, Aug. 1980, doi: 10.1109/tei.1980.298259.

[23] [Online]. Available: https://www.ashrae.org/technical-resources/bookstore/ashrae-international-weather-files-for-energy-calculations-2-0-iwec2

[24] D. L. King, W. E. Boyson, and J. A. Kratochvil, "Photovoltaic array performance model," Sandia National Lab., Albuquerque, NM, USA, Rep. SAND2004-3535, 2004.

[25] *Standard Tables for Reference Solar Spectral Irradiances: Direct Normal and Hemispherical on 37 Tilted Surface*, ASTM G173-03, 2012.

[26] *Photovoltaic Devices - Part 3: Measurement Principles for Terrestrial Photovoltaic (PV) Solar Devices With Reference Spectral Irradiance Data*, IEC 60904-3 ED. 4.0, 2019.

[27] *Standard Practice for Xenon Arc Exposure Test With Enhanced Light and Water Exposure for Transportation Coatings*, ASTM D7869-13, 2013.

[28] M. D. Kempe et al., "Field testing of thermoplastic encapsulants in high-temperature installations," *Energy Sci. Eng.*, vol. 3, no. 6, pp. 565–580, 2015, doi: 10.1002/ese3.104.

[29] M. D. Kempe, D. Holsapple, K. Whitfield, and N. Shiradkar, "Standards development for modules in high temperature micro-environments," *Prog. Photovolt., Res. Appl.*, vol. 29, no. 4, pp. 445–460, 2021, doi: 10.1002/pip.3389.

[30] M. D. Kempe, "Evaluation of the uncertainty in accelerated stress testing," in *Proc. IEEE 40th Photovolt. Spec. Conf.*, 2014, pp. 2170–2175, doi: 10.1109/PVSC.2014.6925355.